S Lazerson et al.

Error field measurement, correction and heat flux balancing on Wendelstein 7-X

Error field measurement, correction and heat flux balancing on Wendelstein 7-X [*]

S. Lazerson[1], M. Otte[2], M. Jakubowski[2], B. Israeli[3], G. Wurden[4], U. Wenzel[2], T. Andreeva[2], S. Bozhenkov[2], C. Biedermann[2], G. Kocsis[5], T. Szepesi[5], J. Geiger[2], T. S. Pedersen[2], D. Gates[1] and the W7-X Team[2]

[1]Princeton Plasma Physics Laboratory, Princeton NJ, 08543, USA
[2]Max-Planck-Institut für Plasmaphysik, 17491, Greifswald, Germany
[3]Columbia University, New York NY, 10027, USA
[4]Los Alamos National Laboratory, Los Alamos, NM, 87544, USA
[5]Wigner Research Center for Physics, Budapest, Hungary

Corresponding Author: lazerson@pppl.gov

Abstract:

The measurement and correction of error fields in Wendelstein 7-X (W7-X) is critical to long pulse high beta operation, as small error fields may cause overloading of divertor plates. Accordingly, as part of a broad collaborative effort, the detection and correction of error fields on the W7-X experiment has been performed using the trim coil system in conjunction with the flux surface mapping diagnostic and high resolution infrared camera. In the early commissioning phase of the experiment, the trim coils were used to open an n/m=1/2 island chain in a specially designed magnetic configuration. The flux surfacing mapping diagnostic was then able to directly image the magnetic topology of the experiment, allowing the inference of a small $\sim 4\,cm$ intrinsic island chain. The suspected main source of the error field, slight misalignment of the superconducting coils, is then confirmed through experimental modeling using the detailed measurements of the coil positions. Observations of the limiters temperatures in module 5 shows a clear dependence of the limiter heat flux pattern as the perturbing fields are rotated. Plasma experiments without applied correcting fields show a significant asymmetry in neutral pressure (centered in module 4) and light emission (visible, H-alpha, CII, and CIII). Such pressure asymmetry is associated with plasma-wall (limiter) interaction asymmetries between the modules. Application of trim coil fields with n=1 waveform correct the imbalance. Confirmation of the error fields allows the assessment of magnetic fields which resonate with the n/m=5/5 island chain.

1 Introduction

The ability to compensate the effects of error fields in W7-X may be of critical importance to the performance of the experiment [1, 2]. Overloading of the divertor elements from symmetry-breaking error fields would limit the achievable heat exhaust. Thus, error fields which resonate with the $\iota = 1$ surface and break the $n/m = 5/5$ symmetry of the divertor island chain are of great interest.

A series of experiments durring the first experimental campaign on W7-X made use of the trim coil [3, 4]. These coils provided by correcting and perturbing magnetic fields. A $n/m = 1/2$ island chain was generated during the flux surface mapping campaign [5]. The effect of error fields on limiter heat loads were also explored with the trim coils. A high resolution infrared camera [6, 7] gave detailed imagery of the limiters during the pulse. Low limiter temperatures limited the range of diagnostic coverage during this first campaign. However, a compensation capability was demonstrated using the neutral pressure gauges [8]. The capability to symmetrize plasma-wall interactions was demonstrated using the trim coil system.

Metrology of the superconducting coil system provides a detailed model of error fields which arise from coil mis-alignment [9, 10]. These detailed measurements can be used to perform load analysis on the coil where pre-loading, dead-weight, thermal contraction, and electromagnetic loads can be assessed. This may then be input to magnetic field line tracing codes and compared against experimental measures. Section 2, reviews the measurements made during this first experimental campaign on W7-X. Section 3, reviews the effects of coil geometry on modeling, and in the final section predictions for OP1.2 are made.

2 Measurements

Flux surface measurements provided the first detection of error fields and the effects of electromagnetic load on coil geometry. During the imaging of the $n/m = 5/6$ island chain in the OP1.1 limiter configuration, a dependence of the position with respect to field strength was detected [11]. Specifically a radial motion of the island island chain as the field strength was increased. The presence of a $n/m = 4/5$ island chain suggests that resonant field harmonics were present in the device.

A direct measurement of error fields in the experiment was also made possible through flux surface mapping and the $\iota = 1/2$ magnetic configuration [5]. This low-field configuration possessed an $\iota = 1/2$ surface at the mid-radius of the configuration. The $n/m = 1/2$ island chain would only be present if error fields were also present in the experiment. While direct measurement of the intrinsic error field was not possible (technical limitations), the trim coils were used to open an island chain which was imaged. Through analysis of the island width as a function of applied trim coil amplitude and phase, it was possible to extrapolate that a $\sim 4\ cm$ intrinsic island chain was present.

Experiments investigating the effect of the trim coils on plasma-limiter interactions were performed during the first experimental campaign. The effect of a perturbing $n = 1$

trim coil field on the limiter temperatures was examined. In figure 1 a stereotypical limiter IR camera image is shown [6, 7]. Three lines are drawn across the limiter from which temperature data is extracted. The data is analyzed for a series of discharges in which the phase of the $n = 1$ trim-coil waveform is rotated at $1\ kA$ peak coil current. Fitting an sine curve to this data indicates that the phase of the error field is located between modules two and three. Thus compensation should be achieved with phases centered around module five. This is in agreement with flux surface measurements of the $n = 1$ error field. Deteriorating plasma performance prevented a meaningful amplitude scan, except to suggest that at $1\ kA$ peak current the system was overcompensated.
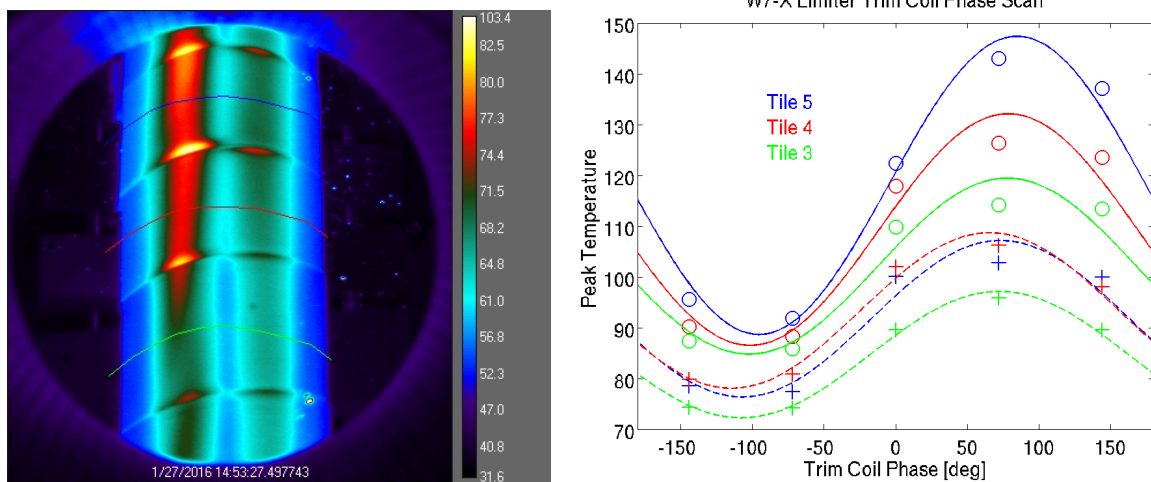

FIG. 1: *Limiter IR camera image (left) and dependence of limiter temperatures on applied trim coil phase at 1000 A (right). Temperatures on the left hand side (o) and right hand side (+) are plotted, along with $n = 1$ fits to the data.*

The trim coils were also used to demonstrate the ability to compensate error fields in concert with the neutral pressure manometer system [8]. Specifically, an asymmetry in the neutral pressures between modules was present. It is hypothesized that this may be due to plasma-wall interactions. Figure 2 shows the effect of rotating the $n = 1$ trim coil field on the manometer measurements. A clear symmetrization is achieved when the field is aligned with module five (-72°). This is in agreement with previous measurements of the error field phase.

3   Modeling

Five non-planar and two planar coils compose the superconducting coil set of W7-X (over a half field period) [12]. Thus the device has 70 superconducting coils along with the five copper trim coils (mounted outside the cryostat). Slight manufacturing defects in the coils are a source of error fields in the experiment [9, 10]. These defects were addressed during assembly by careful positioning of the coils so as to minimize the unwanted components
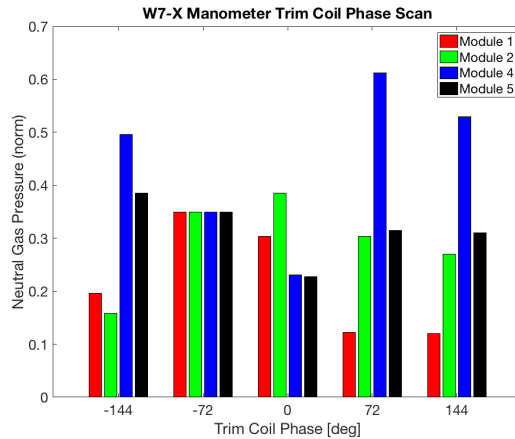
FIG. 2: *Dependence of manometer pressures as a function of applied trim coil $n = 1$ magnetic field. All runs performed at 1000 A peak coil current.*

of this source of error field. The weight, cooling, and electromagnetic loads cause elastic deformations of the coils. Detailed measurements of the coils ('as-built') and finite element modeling ('FEM') provide a more accurate representation of these effects. Effects which are not present in the design basis model ('CAD'). Both the 'CAD' and 'as-built' models of the coils have been interfaced to magnetic field line tracing codes for analysis, along with 'FEM' load analyzed versions of both.
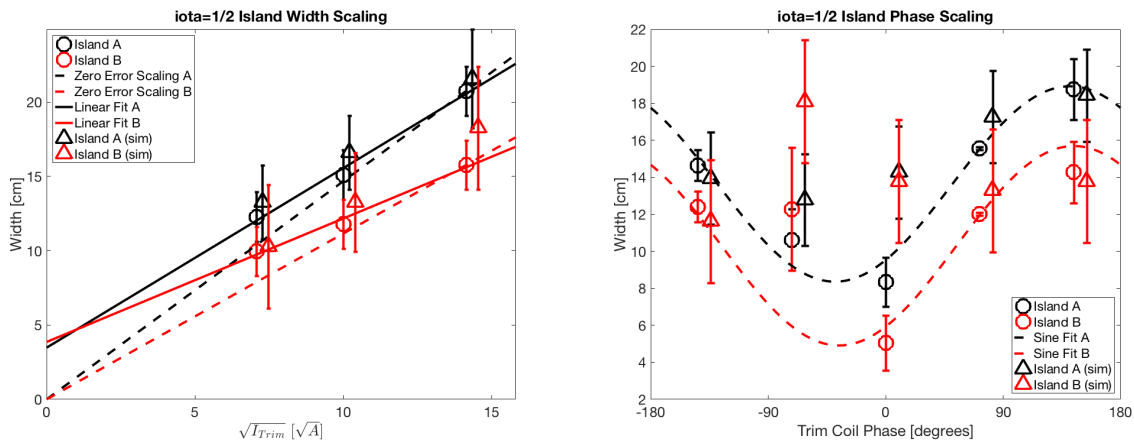

FIG. 3: *Simulated (triangle) and experimental (o) data for trim coil amplitude and phase scans. Simulations were preformed using the 'as-built' W7-X coil set. Simulated data points have been shifted right slightly to aid in visualization.*

Simulations of the $\iota = 1/2$ magnetic configuration using the various coil models provide confirmation of the source of the error fields. As it was used in the design of the configuration, the 'CAD' coil model indicates no significant island presence at the $n/m = 1/2$

rational surface. The 'as-built' coil model indicated the presence of an $\sim 4\ cm\ n/m = 1/2$ island chain at the rational surface. Figure 3 depicts simulations using this coil set alongside the experimental data. The agreement between simulation and experiment confirms that the error field in W7-X is primarily arising from coil mis-alignment and manufacturing defects. This analysis neglected the 'FEM' analysis because the experiment was carried out at relatively low magnetic field $0.3\ T$. This does however provide confidence in the use of the 'as-built' coil for simulation. The neglect of the electromagnetic loading may account for discrepancies seen in the phase scan.

Elastic deformation of superconducting magnetic system due to electromagnetic loads was observed during flux surface mappings of the OP1.1 limiter configuration. The $n/m = 5/6$ island chain had a radial location which was dependent on the toroidal magnetic field strength. Qualitative agreement is found between the 'CAD-FEM' models and the first five passes of the flux surface mapping electron beam (figure 4). However, the best fit between simulations and experimental images was found at $\sim 60\%$ the actual experimental forces.
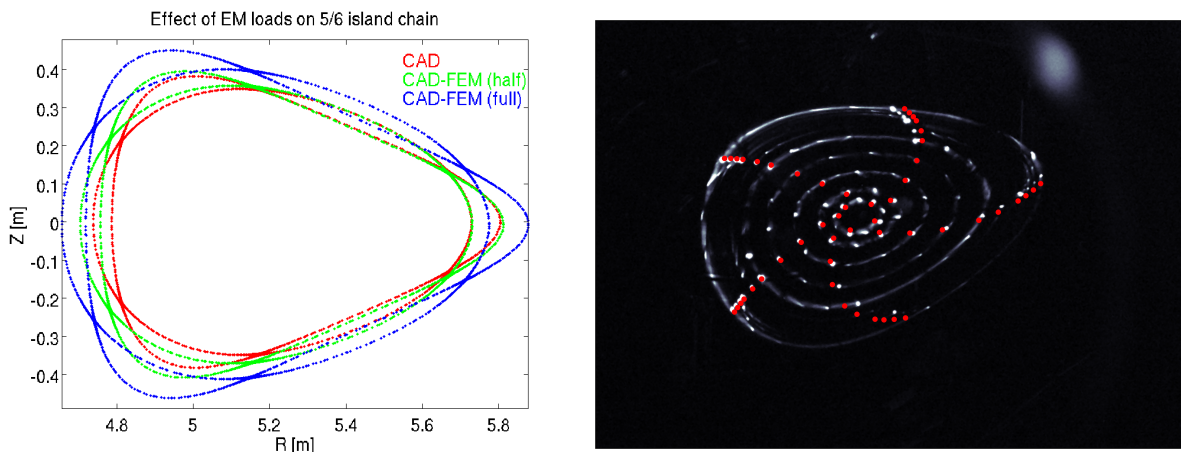

FIG. 4: *Simulations showing the change in 5/6 island position with field strength (left) and best fit of simulation results to experiment (right). Simulations were performed using the 'CAD' coil model at zero, half field, and full field strength (2.5 T). Best fit found for 1.9 T FEM model using first five electron beam passes.*

The limiter connection lengths in the absence of error fields are characterized by three regions [13]. These regions each have a unique connection length to the neighboring limiter or from one side of the limiter to the other (all making at least one full toroidal transit. The error fields, as modeled using the 'as-built-FEM' coil, modify the limiter connection lengths (figure 5). In addition to breaking the field period symmetry of the connection length pattern, long connection length regions appear at the top and bottom of the limiter. Additionally, features near the center of the limiter appear on two of the limiters. This suggests the possibility of additional regions of limiter heat loading.
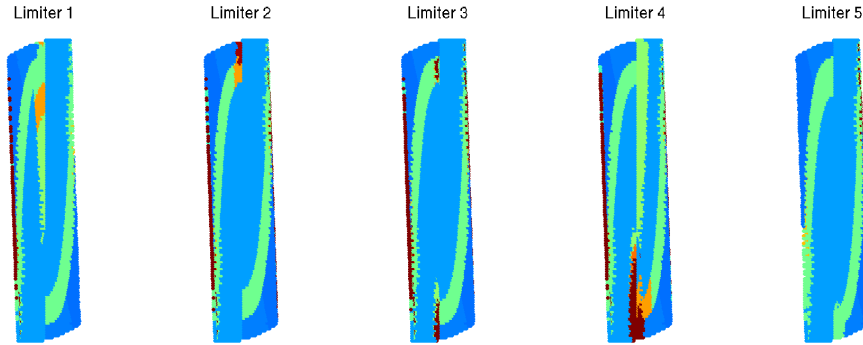
FIG. 5: Limiter connection lengths for the 'as-built-FEM' coil model for all five limiters. Notice that features have appeared at the top and bottom of most limiters.

4 Discussion

The studies of error fields in W7-X performed during the first experimental campaign paint a consistent picture of error fields and their sources in the device. Flux surface mapping, limiter temperatures, and neutral pressure measurements depict a consistent picture of the phase of an $n = 1$ error field. Detailed analysis of flux surface imaging campaign confirms the source of the error fields to be due to slight misalignments of the superconducting magnetic coils. Moreover, these measurements indicate the necessity of mechanical, thermal and electromagnetic load modeling, for accurate depiction of the magnetic field. So while care must be taken in the modeling of these fields, they are well within the limits of trim coils system for compensation.

Looking forward to the next operational campaign, we can now predict with some confidence the role error fields will play. In OP1.1 we were not able to directly measure the $n/m = 1/1$ component of the magnetic field. This will be done in OP1.2 using the 'high-iota' configuration. The 'compass-scan' technique will be used to analyze the helical shift of the W7-X magnetic axis in this configuration. However, the results obtained here already provide confidence that the trim coils will be capable of symmetrizing divertor mis-loading between modules.

Acknowledgements

References

[1] Sergey A Bozhenkov, Joachim Geiger, M Grahl, Johann Kisslinger, A Werner, and R C Wolf. Service oriented architecture for scientific analysis at W7-X. An example of a field line tracer. *Fusion Engineering and Design*, 88(11):2997–3006, November 2013.

[2] Sergey A Bozhenkov, Samuel Lazerson, Matthias Otte, David A Gates, T Sunn Pedersen, and R C Wolf. Methods for measuring 1/1 error field in Wendelstein 7-X stellarator. *Nuclear Fusion*, page 076002, June 2016.

[3] Thomas Rummel, Konrad Riße, Frank Fullenbach, Matthias Koppen, Johann Kisslinger, Tom Brown, Ron Hatcher, Stephen Langish, Mike Mardenfeld, and George Hutch Neilson. The Wendelstein 7-X Trim Coil System. *IEEE Transactions on Applied Superconductivity*, 24(3):1–4, 2014.

[4] T Rummel, K Risse, Johann Kisslinger, M Köppen, F Fullenbach, George Hutch Neilson, Thomas Brown, and S Ramakrishnan. The Trim Coils for the Wendelstein 7-X Magnet System. *IEEE Transactions on Applied Superconductivity*, 22(3):4201704–4201704, 2012.

[5] Samuel Lazerson, Matthias Otte, Sergey Bozhenkov, Christoph Biedermann, Thomas Sunn Pedersen, and the W7-X Team. First measurements of error fields on W7-X using flux surface mapping. *Nuclear Fusion*, page 106005, August 2016.

[6] G A Wurden, L A Stephey, C Biedermann, M W Jakubowski, J P Dunn, M Gamradt, and W7-X Team. A high resolution IR/visible imaging system for the W7-X limiter. *Review of Scientific Instruments*, 87(11):11D607, August 2016.

[7] L Stephey, G A Wurden, O Schmitz, H Frerichs, F Effenberg, C Biedermann, J Harris, R König, P Kornejew, M Krychowiak, E A Unterberg, and W7-X Team. Spectroscopic imaging of limiter heat and particle fluxes and the resulting impurity sources during Wendelstein 7-X startup plasmas. *Review of Scientific Instruments*, 87(11):11D606, August 2016.

[8] Maciej Krychowiak and et al. Overview of diagnostic performance and results for the first operation phase in wendelstein 7-x. Submitted, 2016.

[9] T Andreeva, T Bräuer, M Endler, Johann Kisslinger, and Y Igitkhanov. Analysis of the magnetic field perturbations during the assembly of Wendelstein 7-X. *Fusion Science and Technology*, 46(2):388–394, September 2004.

[10] T Andreeva, T Bräuer, M Endler, Johann Kisslinger, and U v Toussaint. Influence of construction errors on Wendelstein 7-X magnetic configurations. *Fusion Engineering and Design*, 84(2-6):408–412, June 2009.

[11] Matthias Otte, D Aßmus, C Biedermann, Sergey A Bozhenkov, T Bräuer, A Dudek, Joachim Geiger, G Kocsis, Samuel Lazerson, T S Pedersen, F Schauer, T Szepesi, B Standley, and the W7-X Team. Setup and initial results from the magneticflux surface diagnostics at Wendelstein 7-X. *Plasma Physics and Controlled Fusion*, page 064003, May 2016.

[12] Thomas Rummel, Konrad Riße, Gunnar Ehrke, Kerstin Rummel, Andre John, Thomas Monnich, Klaus-Peter Buscher, Walter H Fietz, Reinhard Heller, Olaf Neubauer, and Anatoly Panin. The Superconducting Magnet System of the Stellarator Wendelstein 7-X. *IEEE Transactions on Plasma Science*, 40(3):769–776, 2012.

[13] Thomas Sunn Pedersen, T Andreeva, H S Bosch, Sergey A Bozhenkov, F Effenberg, M Endler, Y Feng, David A Gates, Joachim Geiger, D Hartmann, H Hölbe, M Jakubowski, R König, H P Laqua, Samuel Lazerson, Matthias Otte, M Preynas, O Schmitz, T Stange, Y Turkin, and the W7-X Team. Plans for the first plasma operation of Wendelstein 7-X. *Nuclear Fusion*, pages 1–13, November 2015.